Excited-State Dynamics of Cofacial Pacman Porphyrins

Zhi-Heng Loh, Scott E. Miller, Christopher J. Chang, Scott D. Carpenter, and Daniel G. Nocera*

Department of Chemistry, 6-335, Massachusetts Institute of Technology, 77 Massachusetts Avenue, Cambridge, Massachusetts 02139-4307

Received: July 3, 2002; In Final Form: September 24, 2002

Cofacial palladium(II) bisporphyrins anchored by xanthene [Pd_2(DPX)] and dibenzofuran [Pd_2(DPD)] pillars were prepared, and the dynamics of their triplet excited states were investigated. The phosphorescence quantum yield [$\Phi_p = 4.59(121) \times 10^{-3}$ in CH_2Cl_2] and lifetime [$\tau_p = 18.2(2)$ μs in CH_2Cl_2] of Pd_2(DPD) are significantly attenuated compared to those of its Pd_2(DPX) congener [$\Phi_p = 29.4(5) \times 10^{-3}$ and $\tau_p = 102(3)$ μs in CH_2Cl_2]. Electronic absorption and emission spectroscopy and electrochemical measurements establish that the porphyrin rings of the DPX cofacial analogue are closer to each other than the porphyrin rings of the DPD analogue in fluid solution. These observations are supported by X-ray crystallographic analyses, which show that the metal−metal distance for the dibenzofuran-bridged bisporphyrin in the solid state is almost 3 Å greater than that for bisporphyrins linked by the xanthene spacer. The spectroscopic, photophysical, and structural results suggest that the decreased Φ_p and τ_p of Pd_2(DPD) are not a consequence of simple interplanar interactions but rather arise from the increased conformational flexibility of the porphyrin rings about the aryl ring of the DPD pillar. In support of this contention, the photophysical properties of monomeric palladium etioporphyrin I [Pd(Etio)] and *meso*-phenyl-substituted palladium etioporphyrin II [Pd(PhEtio)] were examined and found to be similar to those of Pd_2(DPX) and Pd_2(DPD), respectively. Density functional theory calculations reveal that torsional motion about the C(*meso*)−C(aryl bridge) bond induces nonplanar distortion of the porphyrin framework, causing a substantial decrease in the T_1-S_0 energy gap. This structural perturbation is consistent with the observed results of enhanced deactivation of Pd_2(DPD) and Pd(PhEtio) triplet excited states.

Introduction

Two metal centers working in concert can promote the multielectron activation of small-molecule substrates. When the bimetallic core has a long-lived excited state, the possibility exists for developing multielectron photochemistry that extends beyond conventional one-electron excited-state pathways.[1−3] Of the various bimetallic complexes capable of supporting multielectron redox chemistry, porphyrins linked in a face-to-face arrangement (cofacial bisporphyrins) are distinguished by their ability to activate small molecules by more than one electron. Cofacial bisporphyrin complexes of several metals, notably cobalt and iron, are electrocatalysts for the reduction of dioxygen by two and four electrons.[4−6] In addition, ruthenium and osmium cofacial bisporphyrins reduce protons by two electrons to dihydrogen[7] and reduce dinitrogen by four and six electrons,[8,9] and electron-deficient congeners are capable of activating C−H bonds.[10] This extensive multielectron chemistry of cofacial bisporphyrins in their ground electronic state presages an equally rich excited-state chemistry. Yet the dynamics of bimetallic cofacial bisporphyrins in electronic excited states and the factors governing their fundamental photophysical properties have not been elaborated. In the absence of a well-defined photophysical framework, it is not surprising that a multielectron photochemistry for cofacial bisporphyrins has yet to evolve.

Cofacial bisporphyrins can be grouped into one of two classes: bisporphyrins linked by two or more flexible strapping units[11−20] and pillared bisporphyrins anchored by a single rigid bridge.[21−33] From the perspective of excited-state design, the face-to-face presentation of porphyrin rings with rigid pillars is more attractive than that with flexible straps because the latter can adopt a slipped conformation wherein the two porphyrin rings are laterally displaced. Increased molecular flexibility imparted by slackened tethers affects the excited-state dynamics of π-delocalized systems.[34−36] Conversely, rigid pillars disfavor ring slippage effects, and distortion of the cofacial platform is constrained to the vertical flexibility of the porphyrin "bite", otherwise known as the Pacman effect.[4,37−40]

Cofacial bisporphyrins juxtaposed by anthracene (DPA)[21,24] and biphenylene (DPB)[22,23] pillars are the traditional Pacman architectures, although knowledge of their photophysics is limited. Recent studies show that the phosphorescence quantum yield and lifetime of Pd_2(DPA) are lower than those of the monomer analogues Pd(TPP) and Pd(OEP) (OEP = 2,3,7,8,12,13,17,18-octaethylporphyrin and TPP = 5,10,15,20-tetraphenylporphyrin).[41] The dynamics responsible for the observed differences in the photophysics of the monomer and cofacial systems have eluded characterization in part because of the arduous synthesis of the necessary precursors for the DPA and DPB pillars. To this end, we have developed new methods for the facile assembly of cofacial bisporphyrins bridged by xanthene (DPX)[38,39,42−45] and dibenzofuran (DPD)[37−39,45] pillars. Not only are the pillars easier to synthesize, but the systems also display vertical pocket sizes spanning over 5 Å in metal−metal distances with little to no lateral displacements. Consequently, the systems are ideal scaffolds for isolating how the Pacman effect, so important to the multielectron catalysis of cofacial porphyrins, is manifested in excited-state dynamics.

10.1021/jp026440p CCC: $22.00
Published on Web 11/08/2002

We report herein a combined structural and spectroscopic investigation of the triplet excited states of palladium(II) DPX and DPD complexes, presenting the most extensive photophysical study to date of pillared cofacial bisporphyrins.[46] The photophysical behavior of these cofacial platforms are compared to the monomer analogues palladium etioporphyrin I, Pd(Etio) (Etio = etioporphyrin I), and *meso*-phenyl-substituted palladium etioporphyrin II, Pd(PhEtio) [PhEtio = 5-(4′-bromophenyl)-2,8,-13,17-tetraethyl-3,7,12,18-tetramethylporphyrin]. The results obtained from steady-state and time-resolved electronic spectroscopy, electrochemistry, and X-ray structural analysis, together with those of density functional theory calculations, identify the critical molecular motions that govern the properties of long-lived excited states of cofacial bisporphyrins. We find that Pacman porphyrins containing cofacial subunits close to van der Waals contact display long-lived triplet excited states. Conversely, those with splayed subunits exhibit strongly quenched phosphorescence as a result of torsional freedom around the bridgehead porphyrin *meso* carbon. This unified excited-state model provides an underpinning for developing the excited-state reaction chemistry of these supramolecular clefts.

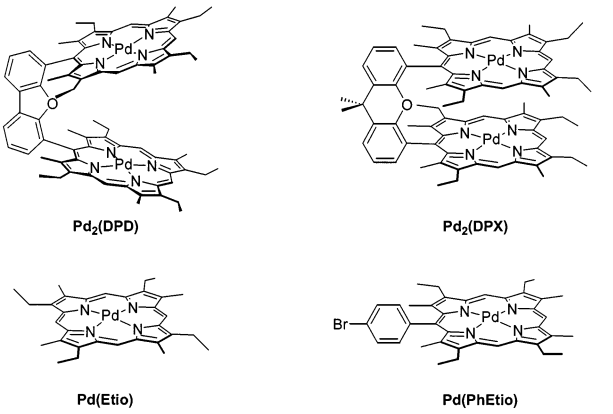

Results and Discussion

Steady-State Spectroscopy. The ground-state electronic absorption spectra of Pd_2(DPX) and Pd_2(DPD) exhibit hypso-type behavior arising from the overlap between filled d_{xz} and d_{yz} orbitals of Pd and empty porphyrin π^* orbitals.[47] An intense Soret band is observed in the UV region with accompanying Q(0,0) and Q(1,0) vibronic bands in the visible region (Figure 1). The absorption maxima and the molar absorption coefficients for the compounds in CH_2Cl_2 are collected in Table 1. The Soret band of Pd_2(DPX) is markedly blue-shifted relative to that of Pd_2(DPD). Conversely, the Q-bands of Pd_2(DPX) are red-shifted relative to those of the DPD analogue. The steady-state phosphorescence spectra of Pd_2(DPX) and Pd_2(DPD) in CH_2Cl_2 are shown in Figure 2, and accompanying phosphorescence maxima (λ_p) and quantum yields (Φ_p) are summarized in Table 1. In accordance with the trend in Q-band energetics, λ_p of Pd_2(DPX) is red-shifted relative to that of Pd_2(DPD); Φ_p of Pd_2(DPX) is larger than that of Pd_2(DPD). The spectral shifts observed for Pd_2(DPX) relative to Pd_2(DPD) are consistent with greater exciton coupling[48] in the former due to the closer spacing of its porphyrinic rings.[49] Because red shifts of the Q-bands due to exciton coupling are usually negated by solvation effects,[50] the pronounced red shift in the Q-bands of Pd_2(DPX) suggests the presence of particularly strong exciton coupling.

The magnitude of the exciton splitting, V, can be evaluated within a point dipole−point dipole framework[51]

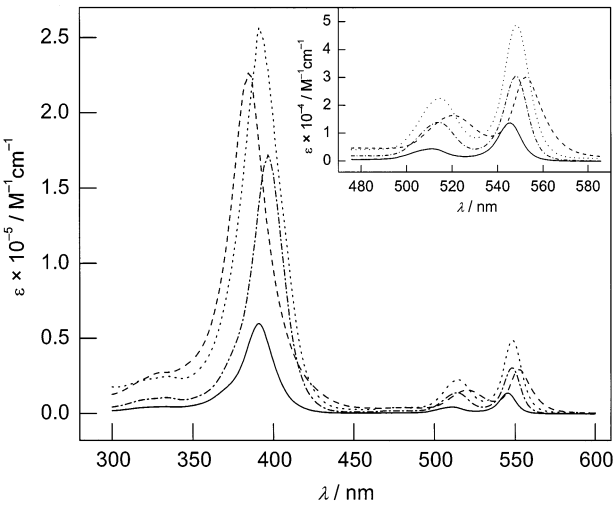

Figure 1. Electronic absorption spectra of Pd(Etio) (—), Pd(PhEtio) (- · - · - ·), Pd_2(DPX) (- - -), and Pd_2(DPD) (· · ·) in CH_2Cl_2 at 298 K.

TABLE 1: Steady-State Spectroscopic Data and Phosphorescence Lifetimes for Palladium(II) Porphyrins in CH_2Cl_2 at 298 K

	λ_{abs}/nm ($\epsilon \times 10^{-3}$/M^{-1}·cm^{-1})					
	B(0,0)	Q(1,0)	Q(0,0)	λ_p/nm	$\Phi_p \times 10^3$	τ_p/μs
Pd_2(DPX)	386 (223)	521 (16)	552 (30)	678	29(1)	102 (3)
Pd_2(DPD)	391 (256)	515 (23)	548 (49)	673	4.6(12)	18.2 (2)
Pd(Etio)	391 (60)	511 (4.4)	546 (14)	669	64(4)	321 (12)
Pd(PhEtio)	397 (176)	515 (14)	548 (31)	673	0.72(5)	1.14 (1)

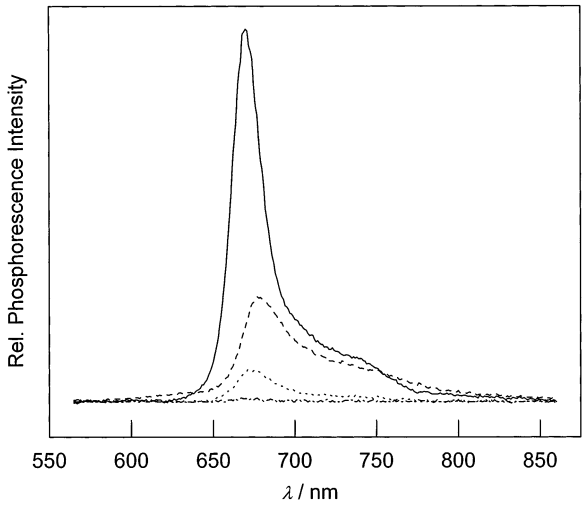

Figure 2. Steady-state phosphorescence spectra of Pd(Etio) (—), Pd-(PhEtio) (- · - · - ·), Pd_2(DPX) (- - -), and Pd_2(DPD) (· · ·) in CH_2Cl_2 at 298 K.

$$V = (e^2 M_i M_j / R^3) F_g \quad (1)$$

where M_i and M_j are the transition dipole lengths of interacting cofacial molecular subunits i and j, respectively; R is the center-to-center distance between them; and F_g is a geometric factor. M can be obtained from spectroscopic data by[52]

$$M^2 = \frac{\epsilon_{max}}{2500\, G} \frac{\delta\lambda}{\lambda_{max}} \quad (2)$$

where ϵ_{max} is the molar absorption coefficient, G is the degeneracy of the spectroscopic state, $\delta\lambda$ is the full-width at half-maximum of the absorption band, and λ_{max} is the absorption maximum. F_g is given by

$$F_g = \cos\alpha - 3\cos\phi_i \cos\phi_j \quad (3)$$

where α is the angle between transition dipole moments $\vec{\mu}_i$ and $\vec{\mu}_j$ (i.e., interplanar angle between cofacial rings), and ϕ_i and ϕ_j are the respective angles between the transition dipole vectors and the vector $\vec{R}$ (i.e., the center-to-center line). The Soret band ($S_2 \leftarrow S_0$) of the cofacial porphyrins was subject to this analysis. From metrical parameters deduced from single-crystal X-ray structural analysis of the porphyrin dimers (vide infra), exciton splittings for Pd_2(DPX) and Pd_2(DPD) in CH_2Cl_2 are calculated to be 5950 and 1410 cm^{-1}, respectively. These values consider only electronic effects; solvent stabilization of the cofacial excited state has been ignored. Because the solvent stabilization effect can be significant, serving to stabilize the S_2 excited state,[49,50] the calculated exciton splittings exceed the observed spectral shifts of the B(0,0) band of Pd_2(DPX) and Pd_2(DPD) [as measured relative to the monomer Pd(PhEtio) in Table 1].

With the aim of evaluating how the aryl ring of the DPX and DPD pillars contributes to the electronic properties of Pd_2(DPX) and Pd_2(DPD), the absorption and phosphorescence properties of the monomer analogues Pd(Etio) and Pd(PhEtio) were investigated. As displayed by Figure 1, the Soret and Q-bands of Pd(PhEtio) shift to lower energy relative to those of Pd(Etio); absorption maxima and molar absorption coefficients are collected in Table 1. The observed red-shift in the Pd(PhEtio) spectrum is ascribed to the introduction of a phenyl group at the *meso* position, which increases the energy of the highest occupied molecular orbital (HOMO) by raising the energy of the a_{2u} orbital above that of the a_{1u} orbital.[53] Moreover, the Soret band of Pd(PhEtio) lies at lower energy than the Soret bands of Pd_2(DPX) and Pd_2(DPD). This result is consistent with the observation of exciton coupling between porphyrin subunits of cofacial Pacman dimers.

Steady-state phosphorescence spectra of Pd(Etio) and Pd(PhEtio) are shown in Figure 2. The results are in accord with absorption spectra. Namely, the phosphorescence maximum tracks the energies of the Q-band absorptions along the series Pd(Etio) < Pd(PhEtio) $\approx$ Pd_2(DPD) < Pd_2(DPX) (Table 1). The Φ_p value of Pd(PhEtio) is smaller than that of Pd(Etio) by 2 orders of magnitude (Table 1).

Electrochemical and Structural Studies. Electrochemical measurements of Pd_2(DPX), Pd_2(DPD), and their monomer analogues support the conclusions drawn from steady-state electronic spectra. Table 2 lists the redox potentials of the palladium(II) porphyrin systems. All four systems exhibit a single, reversible one-electron reduction process. The Pd_2(DPD) complex and the monomers display a single two-electron oxidation wave at similar potentials, suggesting that the porphyrinic subunits in the DPD system are too far apart to perturb each other electronically. In contrast, the Pd_2(DPX) congener exhibits two reversible one-electron oxidation processes. The splitting of the oxidation wave, which is also observed for cobalt cofacial bisporphyrins,[44,54] originates from strong interactions between two proximate porphyrin π systems. Electronic repulsion between the two porphyrin planes results in lowering of $E_{ox}(1)$ from $+0.93 \pm 0.02$ V for the electronically isolated palladium(II) porphyrins to $+0.65$ V in Pd_2(DPX). The value of $E_{ox}(2)$ of Pd_2(DPX) is similar to the $E_{ox}(1)$ value of Pd_2(DPD); this observation is consistent with that made by Collman and co-workers for their group 2 porphyrin dimers.[55] These results provide further evidence for greater electronic coupling between macrocyclic subunits in the more closely packed DPX system relative to the splayed DPD congener.

The X-ray crystal structures of Pd_2(DPX) and Pd_2(DPD), shown in Figures 3 and 4, respectively, concur with spectroscopic and electrochemical studies. The structure of Pd_2(DPX) confirms the compressed nature of the DPX framework with parallel porphyrin rings (interplanar angle = 3.9°). The Pd−Pd distance of 3.97 Å is comparable to the distance of 3.4−3.6 Å required for significant van der Waals overlap between two porphyrin planes.[56,57] In contrast, Pd_2(DPD) presents two porphyrin subunits in a splayed arrangement with a significantly greater bite site (interplanar angle = 11.0°). In this case, the Pd−Pd distance is expanded to 6.81 Å. For both systems, the rigid cyclic ether bridge holds the two porphyrin macrocycles in a face-to-face geometry with minimal lateral displacements; the torsional twists are 14.6° and 3.5° for Pd_2(DPX) and Pd_2(DPD), respectively. Trends in bond lengths and angles of macrocyclic core structures and side chains agree well with those observed in related cofacial bisporphyrins. Complete crystallographic data are provided in the Supporting Information. With

TABLE 2: Cyclic Voltammetric Data for Palladium(II) Porphyrins in CH_2Cl_2 at 298 K Referenced against a Ag/AgCl Electrode

	E/V (ΔE_p/mV)		
	$E_{ox}(1)$	$E_{ox}(2)$	$E_{red}(1)$
Pd_2(DPX)	+0.65 (100)	+0.92 (100)	−1.70 (110)
Pd_2(DPD)	+0.91 (90)	−	−1.49 (100)
Pd(Etio)	+0.95 (150)	−	−1.51 (110)
Pd(PhEtio)	+0.93 (130)	−	−1.51 (110)

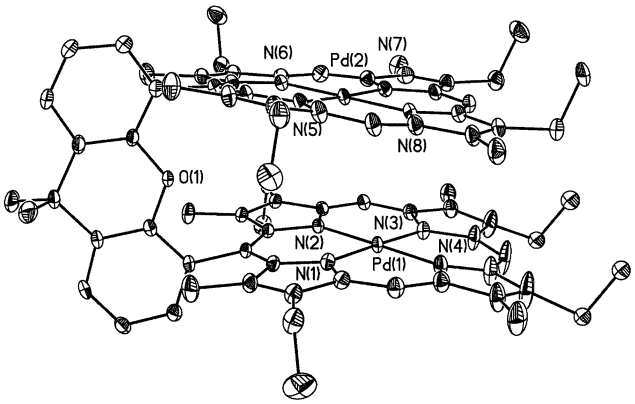

Figure 3. X-ray crystal structure of Pd_2(DPX). Thermal ellipsoids are drawn at the 25% probability level. Hydrogen atoms have been omitted for clarity.

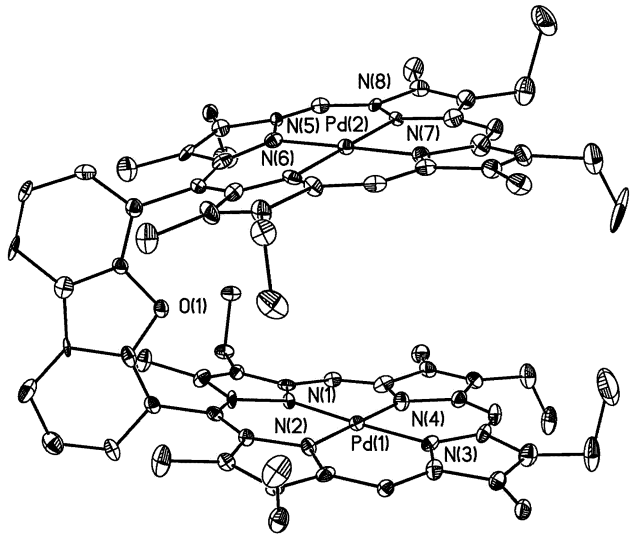

Figure 4. X-ray crystal structure of Pd_2(DPD). Thermal ellipsoids are drawn at the 25% probability level. Hydrogen atoms have been omitted for clarity.

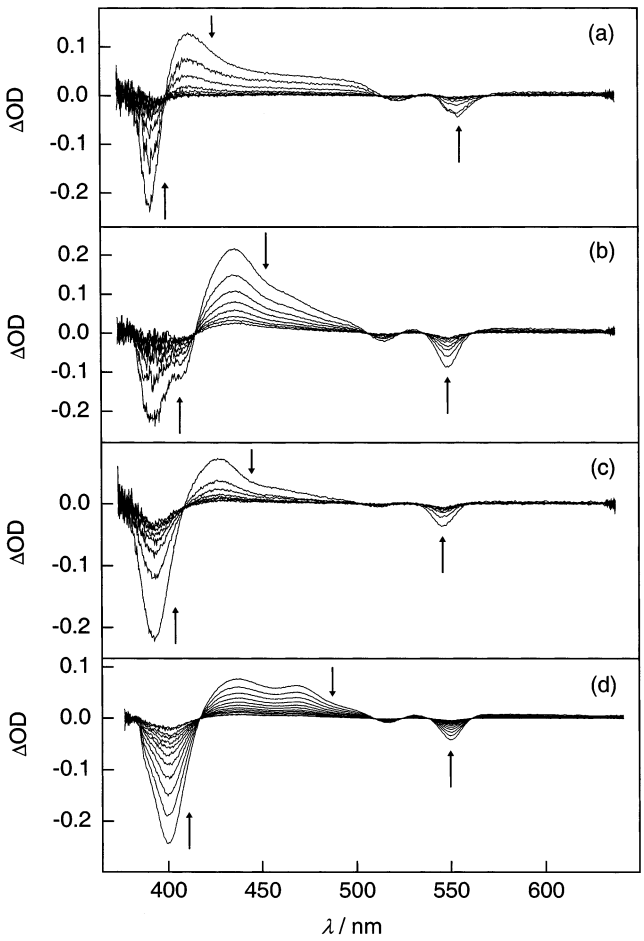

Figure 5. Transient absorption spectra of (a) Pd_2(DPX), (b) Pd_2(DPD), (c) Pd(Etio), and (d) Pd(PhEtio) in CH_2Cl_2 at long time scales. Spectra were collected at time intervals of 50 μs for Pd_2(DPX) and Pd(Etio), 5 μs for Pd_2(DPD), and 200 ns for Pd(PhEtio).

a firm understanding of the structure and steady-state spectroscopy of the palladium porphyrin monomers and dimers in hand, we turned our attention to time-resolved spectroscopic studies so that we could directly examine the excited-state dynamics of the Pacman systems.

Time-Resolved Spectroscopy. The speciation of the long-lived excited states of palladium porphyrin monomers and dimers was examined using nanosecond transient absorption spectroscopy. Figure 5 depicts transient absorption spectra following a 5-ns excitation pulse at 550 nm. The four palladium porphyrin compounds display similar profiles. A prominent, broad absorption feature is observed between the bleaching signals of the Soret and Q(1,0) bands. In addition, the Q(0,0) bleach is also observed to the red of the Q(1,0) bleach. Attendant excited-state absorptions are observed to the low-energy side of the Q-bands. The energetic trends of these transient features track the corresponding ground-state electronic absorption spectra. The triumverate of Pd_2(DPX), Pd_2(DPD), and Pd(Etio) each exhibit one prominent absorption maximum at 412, 435, and 427 nm, respectively, in addition to a low-energy shoulder. In Pd(PhEtio), the secondary absorption maximum at 468 nm is clearly apparent to the low-energy flank of the primary absorption at 436 nm.

The transient absorption spectra of Pd_2(DPX), Pd_2(DPD), and Pd(Etio) decay monoexponentially to ground state on the microsecond time scale, indicative of an excited state with pronounced triplet character. The susceptibility of these transient species to quenching by O_2 further confirms a triplet origin.

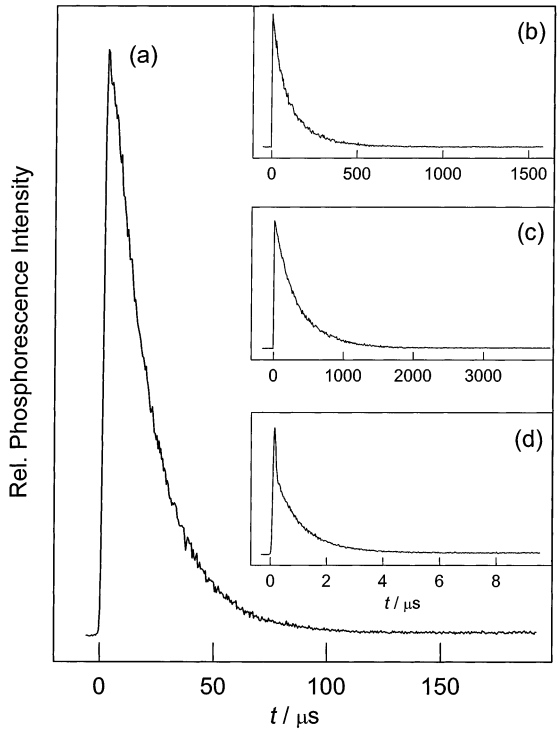

Figure 6. Time-resolved phosphorescence decays of (a) Pd_2(DPD), (b) Pd_2(DPX), (c) Pd(Etio), and (d) Pd(PhEtio) in CH_2Cl_2. Vertical and horizontal axes of insets refer to phosphorescence intensity and time (in microseconds), respectively. The initial spike in the decay of Pd(PhEtio) is instrument-limited and is due to white light generation in the sample.

Moreover, concomitant recovery of the Soret and Q-band bleaches on the same time scale as the excited-state absorption decay establishes the absence of any intermediates in the deactivation of this triplet excited state.

Pd(PhEtio) is distinguished from the other palladium(II) porphyrins by the two absorption maxima. The transient decays of the two bands are dominated by a 1.10(7)-μs component. The occurrence of two maxima in the transient absorption spectrum of Pd(PhEtio) suggests the presence of two triplet states. This result is in accordance with Albinsson's observation of a "mother−daughter" relationship for two triplet excited states of zinc *meso*-diaryloctaalkyl porphyrins. The mother signal arises from a porphyrin in a planar geometry and the daughter signal arises from a porphyrin macrocycle that exhibits a nonplanar distortion.[58] Along these lines, the presence of two triplet absorption bands in the transient spectrum of Pd(PhEtio) suggests planar and nonplanar geometries for the excited state.

Because the palladium(II) porphyrin monomers and dimers decay directly to their respective singlet ground states with no detectable intermediates, phosphorescence lifetime (τ_p) measurements can be employed to unravel the excited-state dynamics of the palladium porphyrins. The time-resolved phosphorescence decays for Pd_2(DPX) and Pd_2(DPD) in CH_2Cl_2 are shown in Figure 6, and their τ_p values are collected in Table 1. These lifetimes are entirely consistent with the decay lifetimes measured from transient absorption decays. Two striking results emerge from the data in Table 1: (i) the monoexponential excited-state decays of Pd_2(DPX) and Pd_2(DPD) occur on markedly disparate time scales [τ_p = 102(3) μs and 18.2(2) μs for DPX and DPD, respectively], and (ii) Pd(Etio) exhibits a long excited-state lifetime [τ_p = 321(12) μs] resembling the Pd_2(DPX) system, whereas Pd(PhEtio) is more similar to Pd_2(DPD), displaying a phosphorescence decay with a τ_p value of

1.14(1) μs. Moreover, the long τ_p of Pd_2(DPX) is comparable to that of Pd_2(DPA) [τ_p = 230(50) μs in 2-MeTHF] and monomeric Pd(TPP) [τ_p = 230(50) μs in 2-MeTHF],[41] and the trend in phosphorescence lifetimes of the palladium(II) porphyrin monomers and dimers correlate with Φ_p. That is, the Φ_p values of Pd_2(DPD) and Pd(PhEtio) are substantially smaller than those of their Pd_2(DPX) and Pd(Etio) counterparts. These collective results reveal that the phosphorescence lifetimes and quantum yields of bisporphyrins at van der Waals contact are not significantly perturbed by the cofacial Pacman arrangement.

On the Molecular Origin of the Excited-State Decay Pathways of Pacman Porphyrins. Antipas and Gouterman previously proposed that the phosphorescence quantum yields and lifetimes of porphyrins containing second- and third-row transition metals are determined by the $d_\pi-e_g(\pi^*)$ energy gap and the heavy metal effect.[59] In particular, an increase in the $d_\pi-e_g(\pi^*)$ energy gap results in less mixing of d orbital character into the $e_g(\pi^*)$ molecular orbital, thus decreasing spin−orbit coupling of and radiative and nonradiative decay from the triplet excited state. The energy gap argument is plausibly applicable to the analysis of our results, given that exciton coupling is expected to produce a larger T_1-S_0 energy gap in Pd_2(DPX) than in Pd_2(DPD)[60] and that phosphorescence from Pd_2(DPX) is less strongly quenched than that from Pd_2(DPD). However, the monomeric Pd(Etio) compound exhibits a phosphorescence lifetime and quantum yield that are similar to those of Pd_2(DPX). For this reason, the correlation of phosphorescence lifetimes and quantum yields of Pacman systems with exciton coupling is untenable. Additionally, electrochemical measurements confirm that the intramolecular charge-separated states for the palladium(II) porphyrins lie too high in energy ($E_{CS} \approx 2.4$ eV) to serve as a deactivation pathway for the porphyrin triplet excited state ($E_T \approx 1.8$ eV). Nanosecond transient absorption studies also demonstrate that there are no intermediate states involved in the triplet excited-state decays. Thus, the enhanced phosphorescence quenching observed for Pd_2(DPD) and Pd(PhEtio) is unlikely to be induced by the participation of lower-lying excited states, suggesting that DPD/PhEtio porphyrins can undergo nonradiative decay processes that are not available to DPX/Etio congeners. This contention is supported by extraction of the nonradiative decay rate constants from Φ_p and τ_p. From the data in Table 1, the k_{nr} rate constants of Pd_2(DPD) and Pd(PhEtio) are 5.5×10^4 and 8.8×10^5 s^{-1}, respectively, as compared to 9.5×10^3 and 2.9×10^3 s^{-1} for Pd_2(DPX) and Pd(Etio), respectively. We note that this calculation assumes that the $S_1 \rightarrow T_1$ intersystem crossing efficiency is unity.

In addressing the issue of additional nonradiative decay pathways in Pacman porphyrins, we were struck by the fact that the presence of a single *meso*-phenyl ring on a palladium(II) macrocycle leads to large differences in the photophysics of the monomer and that transient absorption results suggest planar and nonplanar excited-state geometries for the Pd(PhEtio) macrocycle (vide supra). Accordingly, we became interested in examining the suggestion by Knyukshto et al.[61] that aryl rings on octaalkyl porphyrin macrocycles are associated with unique nonradiative decay pathways. Density functional theory (DFT) calculations were undertaken to investigate the effect of torsional motion about the C(*meso*)−C(phenyl) bond on both geometry and electronic structure. *Meso*-phenyl-substituted palladium(II) etioporphyrin was structurally simplified by substituting all four ethyl groups with methyl groups to give *meso*-phenyl-substituted palladium(II) 2,3,7,8,12,13,17,18-octamethylporphyrin, Pd(PhOMP).

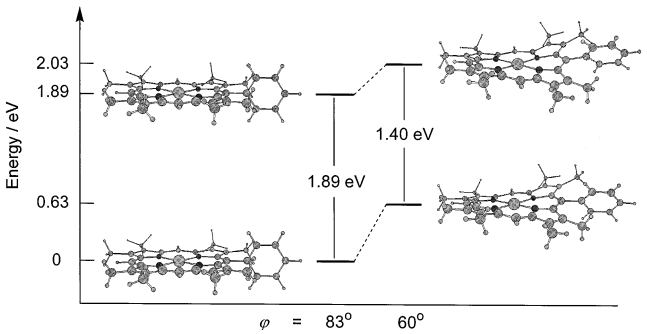

Figure 7. Energy level diagram showing the relative energies of both singlet and triplet states of Pd(PhOMP) on going from the planar structure to the distorted structure. The DFT-optimized structures of planar and distorted Pd(PhOMP) in both singlet and triplet states are also shown; φ is the torsional angle between the porphyrin plane and the *meso*-phenyl substituent. The value of the T_1-S_0 energy gap upon nonplanar distortion is depicted between the HOMO and LUMO levels.

Figure 7 displays an energy level diagram depicting the relative energies of both singlet and triplet states of Ph(PhOMP). Geometry optimization on the singlet potential energy surface, without any imposed constraints, furnishes a structure in which the porphyrin subunit remains planar and the torsional angle φ between the porphyrin plane and the *meso*-phenyl substituent is found to be 83°. Geometry optimization on the triplet potential energy surface affords a similarly planar macrocycle, in which the bond lengths are within 0.01 Å of those in the singlet-state structure. Geometry optimization on both singlet and triplet potential energy surfaces with a constraint of φ = 60° yields similar structures for the two spin states, both of which exhibit pronounced nonplanar distortions. The nonplanar distortions present in these geometries are dominated by saddling and ruffling, with larger distortions occurring in the half of the macrocycle containing the *meso*-phenyl substituent.

Energy gap law considerations relate $T_1 \rightarrow S_0$ decay to the energetic differences between triplet excited and singlet ground electronic states. We find that the T_1-S_0 energy gap decreases from 1.89 to 1.40 eV upon nonplanar distortion of the porphyrin macrocycle. Within the framework of a multiphonon-assisted nonradiative decay,[62−64] a smaller energy gap leads to an increase in the nonradiative decay rate due to enhancement of the Franck−Condon factor.[65−67] Moreover, nonplanar distortion of a porphyrin macrocycle is accompanied by a corresponding increase in one-center overlap integrals between the nitrogen lone pairs and porphyrin π orbitals, further enhancing $T_1 \rightarrow S_0$ intersystem crossing.[68,69] These two factors, decreased energy gap and increased $n-\pi$ orbital mixing, have been invoked by Holten and co-workers to explain anomalously fast nonradiative decay rates from the S_1 state of distorted porphyrins.[70−73] It is reasonable to expect that the same constructs are applicable to the dynamics of the triplet excited state. We believe that the results of Figure 7 translate to the splayed Pacman system owing to the similar photophysical properties of Pd_2(DPD) and Pd(PhEtio). Although the τ_p and Φ_p values for Pd_2(DPD) are not as small as those for Pd(PhEtio), they are clearly divergent from those of cofacial Pd_2(DPX) and Pd_2(DPA) Pacman systems in which the cofacial subunits are in van der Waals contact.

Taking into account the combination of spectroscopic results and DFT calculations, we therefore ascribe the faster triplet excited-state decay of Pd_2(DPD), as compared to Pd_2(DPX), to torsional motion about the C(*meso*)−C(aryl) bond between the porphyrin planes and the aryl of the DPD bridge. The relatively small triplet-state deactivation in Pd_2(DPX) is consistent with the short Pd−Pd distance and the small interplanar angle

between the two porphyrin subunits. These structural elements constrain conformational flexibility about the C(*meso*)−C(aryl bridge) bond of the DPX Pacman.

Concluding Remarks

The successful design and implementation of new molecular catalysts for multielectron photochemical cycles are predicated on a thorough understanding of their excited-state dynamics. Owing to the extensive multielectron chemistry of cofacial Pacman porphyrins in their ground state, we sought to establish a starting point for developing a correspondingly expansive excited-state chemistry. To this end, we examined the triplet excited-state dynamics of cofacial bisporphyrin systems based on xanthene (DPX) and dibenzofuran (DPD), which exhibit large differences in vertical pocket size and flexibility. The significant finding reported herein is that torsional motions about the C(*meso*)−C(aryl) bond contribute greatly to the excited-state dynamics of Pacman systems. The DPX spacer places cofacial porphyrin subunits in van der Waals contact, structurally constraining torsional rotation about the aryl bridge. Accordingly, the phosphorescence lifetime and quantum yield of this system are comparable to those of a simple etioporphyrin. In contrast, the DPD pillar imparts a significantly greater Pacman bite angle between cofacial subunits, resulting in more torsional freedom about the aryl bridge. This enhanced flexibility induces macrocyclic distortion in the excited state, leading to more efficient nonradiative decay.

The combined spectroscopic and theoretical findings provide important insights for the design of multielectron, photocatalytic cycles using cofacial Pacman porphyrins and related platforms. For thermal multielectron reactivity, we have previously demonstrated that the range of vertical flexibility for cofacial bisporphyrins is advantageous for efficient catalysis, allowing for facile substrate access and product release and for large structural changes during the turnover of bond-making and bond-breaking reactions.[38,39,44] However, the photophysical data reported here suggest that these structural attributes might not directly translate to efficient excited-state reactivity. In particular, the significantly reduced phosphorescence lifetime for the splayed DPD framework compared to its compressed DPX counterpart demonstrates that controlling the motions of porphyrin rotation upon photon absorption is critical for tuning excited-state properties and, hence, reactivities. An attractive approach to resolving this issue would be to prebind a substrate to hinder porphyrin rotation. With this longer-lived excited state, more efficient photocatalysis is anticipated for a preorganized system in which the substrate is already situated within the molecular cleft. To this end, we are currently examining the photophysics of supramolecular Pacman constructs rigidified by encapsulated guests.

Experimental Section

Materials. Silica gel 60 (70−230 and 230−400 mesh, Merck) was used for column chromatography. Analytical thin-layer chromatography was performed using Merck 60 F254 silica gel (precoated sheets, 0.2 mm thick). Solvents for synthesis were of reagent grade or better and were dried according to standard methods. Dichloromethane used in spectroscopic measurements was obtained from Burdick & Jackson (spectroscopic grade), whereas methylcyclohexane was obtained from EM Science (AR grade); these solvents were used without further purification. The dipyrrylmethane precursors 5-(4′-bromophenyl)-3,3′-dimethyl-4,4′-diethyl-2,2′-dipyrrylmethane[74] and 3,3′-diethyl-5,5′-diformyl-4,4′-dimethyl-2,2′-dipyrrylmethane[75,76] and the porphyrins H_4(DPX),[42] H_4(DPD),[37] and Pd(Etio)[77] were prepared as described previously. All other reagents were used as received. Mass spectral analyses were carried out at the University of Illinois Mass Spectrometry Laboratory. Elemental analyses were performed at Michigan State University.

5-(4′-Bromophenyl)-2,8,13,17-tetraethyl-3,7,12,18-tetramethylporphyrin [H_2(PhEtio)]. A suspension of 5-(4′-bromophenyl)-3,3′-dimethyl-4,4′-diethyl-2,2′-dipyrrylmethane (3.85 g, 10 mmol) and 3,3′-diethyl-5,5′-diformyl-4,4′-dimethyl-2,2′-dipyrrylmethane (2.86 g, 10 mmol) in methanol (500 mL) was purged with nitrogen for 1 h. A solution of *p*-toluenesulfonic acid (2.5 g) in methanol (20 mL) was added dropwise over a period of 1 h. The resulting red mixture was stirred in the dark under nitrogen for 24 h. Solid *o*-chloranil (2.5 g) was added in one portion, and stirring was continued in air for 24 h. The mixture was taken to dryness, and the remaining solid redissolved in 400 mL of chloroform. A saturated methanolic solution of $Zn(OAc)_2 \cdot 2H_2O$ (20 mL) was added, and the solution was refluxed for 1 h. The solvent was removed, and the remaining residue was purified by flash column chromatography (silica gel, dichloromethane). The first band eluted was collected and vigorously stirred with 6 N HCl (15 mL) for 15 min. The solution was neutralized with a 10% aqueous sodium carbonate solution, and the mixture was stirred for an additional 15 min. The organic phase was separated, washed with water (3 × 50 mL), dried over Na_2SO_4, and taken to dryness. Purification by flash column chromatography (silica gel, dichloromethane) followed by recrystallization from dichloromethane/methanol afforded pure H_2(PhEtio) as a grape purple powder (3.25 g, 51% yield). ^{1}H NMR (500 MHz, $CDCl_3$, 25 °C): δ = 10.18 (s, 2H, meso), 9.97 (s, 1H, meso), 7.97 (d, 2H, ArH), 7.89 (d, 2H, ArH), 4.08 (m, 4H, CH_2), 4.02 (m, 4H, CH_2), 3.65 (s, 6H, CH_3), 2.51 (s, 6H, CH_3), 1.89 (t, 6H, CH_3), 1.77 (t, 6H, CH_3), −3.239 (br s, 1H, NH), −3.323 (br s, 1H, NH). HRFABMS (M^+): calcd for $C_{38}H_{41}N_4Br$ (*m*/*z*), 632.252; found, 632.255.

Pd(PhEtio). To a 50-mL chloroform solution of H_2(PhEtio) (50 mg, 0.079 mmol) was added a solution of $Pd(OAc)_2$ (100 mg) and potassium acetate (100 mg) in 8 mL of methanol. The resulting solution was refluxed for 3 h under nitrogen, and the solvent was removed by rotary evaporation. The crude material was purified by flash column chromatography (silica gel, dichloromethane) followed by recrystallization from dichloromethane/methanol to afford analytically pure Pd(PhEtio) as a brick red solid (49 mg, 86% yield). ^{1}H NMR (500 MHz, $CDCl_3$, 25 °C): δ = 10.11 (s, 2H, meso), 10.05 (s, 1H, meso), 7.95 (d, 2H, ArH), 7.89 (d, 2H, ArH), 4.06 (m, 4H, CH_2), 3.96 (m, 4H, CH_2), 3.60 (s, 6H, CH_3), 2.47 (s, 6H, CH_3), 1.89 (t, 6H, CH_3), 1.74 (t, 6H, CH_3). HRFABMS (M^+): calcd for $C_{38}H_{39}N_4BrPd_2$ (*m*/*z*), 736.139; found, 736.140.

Pd_2(DPX). To a 40-mL chloroform solution of H_4(DPX) (50 mg, 0.043 mmol) was added a solution of $Pd(OAc)_2$ (200 mg) and potassium acetate (200 mg) in 12 mL of methanol. The resulting solution was refluxed for 11 h under nitrogen, and the solvent was removed by rotary evaporation. The crude material was purified by flash column chromatography (silica gel, 1:1 hexanes/dichloromethane to dichloromethane) followed by recrystallization from dichloromethane/methanol to afford analytically pure Pd_2(DPX) as a bright red solid (40 mg, 68% yield). ^{1}H NMR (500 MHz, $CDCl_3$, 25 °C): δ = 9.08 (s, 2H, meso), 8.46 (s, 4H, meso), 7.87 (d, 2H, ArH), 7.23 (t, 2H, ArH), 7.02 (d, 2H, ArH), 4.14 (m, 4H, CH_2), 3.85 (m, 4H, CH_2), 3.57 (m, 4H, CH_2), 3.33 (m, 4H, CH_2), 3.21 (s, 12H, CH_3), 2.26 (s,

12H, CH_3), 2.22 (s, 6H, CH_3), 1.72 (t, 12H, CH_3), 1.42 (t, 12H, CH_3). Anal. Calcd for $C_{79}H_{82}N_8OPd_2$: C, 69.14; H, 6.02; N, 8.16. Found: C, 69.17; H, 5.98; N, 8.12. HRFABMS (M^+): calcd for $C_{79}H_{82}N_8OPd_2$ (*m*/*z*), 1370.468; found, 1370.469.

Pd_2(DPD). To a 50-mL chloroform solution of H_4(DPD) (80 mg, 0.071 mmol) was added a solution of $Pd(OAc)_2$ (180 mg) and potassium acetate (200 mg) in 10 mL of methanol. The resulting solution was refluxed for 6 h under nitrogen, and the solvent was removed by rotary evaporation. The crude material was purified by flash column chromatography (silica gel, 1:1 hexanes/dichloromethane to dichloromethane) followed by recrystallization from dichloromethane/methanol to afford analytically pure Pd_2(DPD) as a cherry red solid (85 mg, 90% yield). ^{1}H NMR (500 MHz, $CDCl_3$, 25 °C): δ = 9.67 (s, 4H, meso), 9.51 (s, 2H, meso), 8.65 (d, 2H, ArH), 7.74 (t, 2H, ArH), 7.66 (d, 2H, ArH), 3.65−3.81 (m, 20H, CH_2), 3.26 (s, 12H, CH_3), 2.36 (s, 12H, CH_3), 1.58 (t, 12H, CH_3), 1.53 (t, 12H, CH_3). Anal. Calcd for $C_{76}H_{76}N_8OPd_2$: C, 68.62; H, 5.76; N, 8.42. Found: C, 69.02; H, 5.90; N, 8.33. HRFABMS (M^+): calcd for $C_{76}H_{76}N_8OPd_2$ (*m*/*z*), 1328.421; found, 1328.422.

General Details of X-ray Data Collection and Reduction. X-ray diffraction data were collected using a Siemens 3 circle diffractometer equipped with a CCD detector. Measurements were carried out at −90 °C using Mo Kα radiation (λ = 0.710 73 Å) that was wavelength-selected with a single-crystal graphite monochromator. Four sets of data were collected using ω scans and a −0.3° scan width. All calculations were performed using a PC workstation. The data frames were integrated to *hkl*/intensity, and final unit cells were calculated using the SAINT v.4.050 program from Siemens. The structures were solved and refined with the SHELXTL v.5.03 suite of programs developed by G. M. Sheldrick and Siemens Industrial Automation, Inc. (1995).

X-ray Structure of Pd_2(DPX). A 0.16 mm × 0.19 mm × 0.61 mm ruby red crystal of rod morphology was obtained from slow diffusion of methanol into a dichloromethane solution of the compound. The crystal was coated at STP and mounted onto a glass fiber. A total of 12 860 reflections were collected in the θ range 2.38−23.26°, of which 8993 were unique (R_{int} = 0.0699). The Patterson method was used to locate the palladium atoms; all remaining atoms were placed using the difference Fourier map. Hydrogen atoms were placed in calculated positions using a standard riding model and were refined isotropically. The largest peak and hole in the difference map were 0.937 and −0.874 eÅ^{-3}, respectively. The least-squares refinement converged normally giving residuals of $R1$ = 0.0412 and $wR2$ = 0.1097, with GOF = 1.065. Crystal data for $C_{79}H_{82}N_8OPd_2$: triclinic, $P\bar{1}$, Z = 2, a = 11.1419(8) Å, b = 14.9325(10) Å, c = 20.8014(14) Å, α = 100.6090(10)°, β = 100.9680(10)°, γ = 102.5440(10)°, V = 3223.5(4) Å^3, ρ_{calc} = 1.420 g/cm^3, $F(000)$ = 1430.

X-ray Structure of Pd_2(DPD). A 0.15 mm × 0.16 mm × 0.27 mm mighty red crystal of plate morphology was obtained from slow diffusion of methanol into a dichloromethane solution of the compound. The crystal was coated at STP and mounted onto a glass fiber. A total of 15 257 reflections were collected in the θ range 2.47−23.28°, of which 10 150 were unique (R_{int} = 0.0236). The Patterson method was used to locate the palladium atoms; all remaining atoms were placed using the difference Fourier map. Hydrogen atoms were placed in calculated positions using a standard riding model and were refined isotropically. The largest peak and hole in the difference map were 2.607 and −0.555 eÅ^{-3}, respectively. The least-squares refinement converged normally giving residuals of $R1$ = 0.0413 and $wR2$ = 0.1292, with GOF = 0.564. Crystal data for $C_{80}H_{86}N_8O_2Pd_2$: monoclinic, $P2(1)$, Z = 2, a = 13.1958(7) Å, b = 20.3976(11) Å, c = 14.8663(8) Å, β = 108.9990(10)°, V = 3783.5(4) Å^3, ρ_{calc} = 1.419 g/cm^3, $F(000)$ = 1664.

Physical Measurements. ^{1}H NMR spectra were collected in $CDCl_3$ (Cambridge Isotope Laboratories) at the M.I.T. Department of Chemistry Instrumentation Facility (DCIF) using either a Mercury 300 or an Inova 500 spectrometer at 25 °C. All chemical shifts are reported using the standard δ notation in parts per million; positive chemical shifts are to higher frequency from the given reference. Unless otherwise stated, all spectroscopic measurements were carried out at room temperature (25 ± 2 °C) on 1 × 10^{-5} M solutions. Samples for spectroscopic measurements were contained within an optical cell equipped with a solvent reservoir and a Starna Cells, Inc., 1-cm-path-length clear fused-quartz cell. The two chambers are isolated from each other by a high-vacuum Teflon valve and from the environment with a second high-vacuum Teflon valve. Samples were degassed by four freeze−pump−thaw cycles (1 × 10^{-5} Torr). UV/visible absorption spectra were recorded on a Spectral Instruments, Inc., 440 CCD array spectrophotometer. Steady-state emission spectra were recorded on a custom-built high-resolution instrument.[78] The emission produced upon excitation at 546 nm was collected with a red-sensitive Hamamatsu R316-02 photomultiplier tube over a wavelength range of 565−860 nm. Phosphorescence quantum yields were measured by the comparative method using zinc tetraphenylporphyrin (ZnTPP) in methylcyclohexane (Φ_{fl} = 0.04) as the standard.[79] Optical densities of solutions used in quantum yield measurements were adjusted to be nearly identical, and a correction formula[80] was employed to correct for the different solvents used. Transient absorption of all porphyrins and phosphorescence lifetimes of Pd(Etio) and Pd_2(DPX) were measured on a nanosecond laser system, whereas lifetimes of Pd_2(DPD) and Pd(PhEtio) were measured on a subpicosecond laser system.

The nanosecond laser system consists of a Coherent Infinity-XPO laser. The third harmonic of the 1064-nm fundamental is used to pump an optical parametric oscillator (OPO) that is tunable throughout the visible region (420−700 nm). The OPO produces laser pulses at a repetition rate of 20 Hz with pulse energies of ∼200 μJ and pulse widths of 5 ns. Transient absorption is performed by exciting the sample at 550 nm (pump pulse) and probing with white light continuum generated by a 75-W xenon arc lamp (probe pulse). The probe pulse is electronically delayed relative to the pump pulse by a DG535 delay generator from Stanford Research Systems, Inc.; the shutters used are Vincent Associates Uniblitz T132 fast shutters. The probe pulse passes through the sample into a SPEX Triax 320 spectrometer and is detected with an Andor Technology DH520-25F-01 ICCD camera thermoelectrically cooled to −40 °C. In this study, transient spectra were collected over a wavelength range of 374−638 nm. Time-resolved emission was performed by exciting the sample at 550 nm and collecting the emission at either 650 or 670 nm. The emission signal was amplified in a Hamamatsu R928 photomultiplier tube attached to the lateral exit of the spectrometer. The output from the photomultiplier tube was channelled into a Lecroy 9384 CM digital oscilloscope. All instruments and electronics in this laser system were controlled by software written in Labview (National Instruments).

The subpicosecond laser system consists of a Coherent/BMI Comet-400S two-stage optical parametric amplifier (OPA). The

OPA generates laser pulses at a repetition rate of 1 kHz and offers wavelength tunability from 475 to 710 nm with pulse energies greater than 20 μJ. The OPA is pumped by a Coherent/BMI Alpha-1000 chirped-pulse regenerative amplifier, which, in turn, is pumped by a 10-W, 1-kHz Nd:YLF laser and seeded by a Coherent Mira femtosecond Ti:sapphire oscillator. The oscillator is pumped by a 5-W cw Coherent Verdi solid-state, frequency-doubled Nd:YVO_4 laser. The modular design allows access to the low power (nanojoules per pulse) oscillator pulses at 76 MHz, as well as the more powerful (near-millijoule per pulse) output from the regenerative amplifier (800 nm, 1 kHz). Pulses from the regenerative amplifier are frequency doubled to give pulses at 400 nm. UV pulses are routinely generated from the OPA output to make the effective range for excitation from less than 240 nm to more than 800 nm. The pulses from the regenerative amplifier can be characterized in real time by a Positive Light SSA single-shot autocorrelator, and they were measured to be 100 fs in duration. Emission lifetimes were measured on a Hamamatsu C4334 Streak Scope streak camera, which was controlled with the high-performance digital temporal analyzer (HPDTA) software provided by Hamamatsu Photonics. This system allows for measurements of lifetimes with a resolution of ~10 ps in a time window up to 1 ms limited by the laser repetition rate. Delays involving long time windows ($\geq$100 ns) were generated by a Stanford Research Systems DG535 delay generator, whereas delays for short time windows ($<$100 ns) were generated by a Hamamatsu C1097-04 delay unit. The streak camera is capable of measuring the rise and decay of fluorescence at every wavelength in a 100-nm window simultaneously, allowing for a direct comparison of the kinetics of different spectral features. In this study, the samples were excited using the 550-nm output from the OPA, and emission was collected with the spectral window centered at 650 nm.

Electrochemical experiments were carried out using a Bioanalytical Systems, Inc. (BAS), CV-50W potentiostat/galvanostat. Cyclic voltammetric measurements were performed in a three-compartment cell using a glassy carbon working electrode, an Ag/AgCl reference electrode, and a platinum-wire auxiliary electrode. A modified Luggin capillary separated the working compartment from the reference electrode. Dichloromethane was used as the solvent, with 0.1 M NBu_4ClO_4 as the supporting electrolyte. The solution in the working compartment of the cell was deaerated by bubbling with nitrogen. The working solutions were prepared by recording the background cyclic voltammograms of the electrolyte solution prior to addition of the solid sample. All potentials are reported vs Ag/AgCl and are not corrected for the junction potential.

Computational Methods. Density functional theory (DFT) calculations were carried out at the local density approximation (LDA) level of theory using the Amsterdam Density Functional program.[81−83] The calculations were performed on a home-built Linux cluster consisting of 12 processors running in parallel. Gradient corrections were introduced using the Becke exchange functional[84] (B) and the Lee−Yang−Parr[85] (LYP) correlation functional. Relativistic corrections were included by using the scalar zero-order regular approximation (ZORA).[86−88] C and H were described by a Slater-type orbital double-ξ basis set augmented by one set of polarization functions. N and Pd were described by a Slater-type orbital triple-ξ basis set augmented by two and one set of polarization functions, respectively. Nonhydrogen atoms were assigned a relativistic frozen core potential, with the shells up to and including 3d for Pd and 1s for C and N treated as core.

Acknowledgment. Z.-H.L. gratefully thanks the M.I.T. Undergraduate Research Opportunities Program (UROP) for support and the National Science and Technology Board (Singapore) for an undergraduate scholarship. C.J.C. acknowledges the National Science Foundation and the M.I.T./Merck Foundation for predoctoral fellowships. This work was supported by grants from the National Science Foundation (CHE-0132680) and National Institutes of Health (GM 47274).

Supporting Information Available: Complete X-ray crystallographic data for Pd_2(DPX) and Pd_2(DPD). This material is available free of charge via the Internet at http://pubs.acs.org.

References and Notes

(1) Nocera, D. G. *Acc. Chem. Res.* **1995**, *28*, 209.
(2) Heyduk, A. F.; Macintosh, A. M.; Nocera, D. G. *J. Am. Chem. Soc.* **1999**, *121*, 5023.
(3) Heyduk, A. F.; Nocera, D. G. *Science* **2001**, *293*, 1639.
(4) Collman, J. P.; Wagenknecht, P. S.; Hutchison, J. E. *Angew. Chem., Int. Ed. Engl.* **1994**, *33*, 1537 and references therein.
(5) Chang, C. K.; Liu, H. Y.; Abdalmuhdi, I. *J. Am. Chem. Soc.* **1984**, *106*, 2725.
(6) Lui, H.-Y.; Abdalmuhdi, I.; Chang, C. K.; Anson, F. C. *J. Phys. Chem.* **1985**, *89*, 665.
(7) Collman, J. P.; Ha, Y.; Wagenknecht, P. S.; Lopez, M. A.; Guilard, R. *J. Am. Chem. Soc.* **1993**, *115*, 9080.
(8) Collman, J. P.; Hutchison, J. E.; Lopez, M. A.; Guilard, R.; Reed, R. A. *J. Am. Chem. Soc.* **1991**, *113*, 2794.
(9) Collman, J. P.; Hutchison, J. E.; Ennis, M. A.; Lopez, M. A.; Guilard, R. *J. Am. Chem. Soc.* **1992**, *114*, 8074.
(10) Collman, J. P.; Fish, H. T.; Wagenknecht, P. S.; Tyvoll, D. A.; Chng, L.-L.; Eberspacher, T. A.; Brauman, J. I.; Bacon, J. W.; Pignolet, L. H. *Inorg. Chem.* **1996**, *35*, 6746.
(11) Collman, J. P.; Elliot, C. M.; Halbert, T. R.; Tovrog, B. S. *Proc. Natl. Acad. Sci. U.S.A.* **1977**, *74*, 18.
(12) Chang, C. K.; Kuo, M. S.; Wang, C. B. *J. Heterocycl. Chem.* **1977**, *14*, 943.
(13) Chang, C. K. *J. Heterocycl. Chem.* **1977**, *14*, 1285.
(14) Ichimura, K. *Chem. Lett.* **1977**, 641.
(15) Kagan, N. E.; Mauzerall, D.; Merrifield, R. B. *J. Am. Chem. Soc.* **1977**, *99*, 5484.
(16) Ogoshi, H.; Sugimoto, H.; Yoshida, Z. *Tetrahedron Lett.* **1977**, *18*, 169.
(17) Paine, J. B., III; Dolphin, D.; Gouterman, M. *Can. J. Chem.* **1978**, *56*, 1712.
(18) Cowan, J. A.; Sanders, J. K. M. *J. Chem. Soc., Chem. Commun.* **1985**, 1213.
(19) Anderson, S.; Anderson, H. L.; Sanders, J. K. M. *Acc. Chem. Res.* **1993**, *26*, 469.
(20) Karaman, R.; Bruice, T. C. *J. Org. Chem.* **1991**, *56*, 3470.
(21) Chang, C. K.; Abdalmuhdi, I. *J. Org. Chem.* **1983**, *48*, 5388.
(22) Chang, C. K.; Abdalmuhdi, I. *Angew. Chem., Int. Ed. Engl.* **1984**, *23*, 164.
(23) Collman, J. P.; Hutchison, J. E.; Lopez, M. A.; Tabard, A.; Guilard, R.; Seok, W. K.; Ibers, J. A.; L'Her, M. *J. Am. Chem. Soc.* **1992**, *114*, 9869.
(24) Guilard, R.; Lopez, M. A.; Tabard, A.; Richard, P.; Lecomte, C.; Brandes, S.; Hutchison, J. E.; Collman, J. P. *J. Am. Chem. Soc.* **1992**, *114*, 9877.
(25) Collman, J. P.; Ha, Y. Y.; Guilard, R.; Lopez, M. A. *Inorg. Chem.* **1993**, *32*, 1788.
(26) Le Mest, Y.; Inisan, C.; Laouenan, A.; L'Her, M.; Talarmain, J.; El Khalifa, M.; Saillard, J. Y. *J. Am. Chem. Soc.* **1997**, *119*, 6905.
(27) Harvey, P. D.; Proulx, N.; Martin, G.; Drouin, M.; Nurco, D. J.; Smith, K. M.; Bolze, F.; Gros, C. P.; Guilard, R. *Inorg. Chem.* **2001**, *40*, 4134.
(28) Chardon-Noblat, S.; Sauvage, J. P.; Mathis, P. *Angew. Chem., Int. Ed. Engl.* **1989**, *28*, 593.
(29) Senge, M. O.; Gerzevske, K. R.; Vicente, M. G. H.; Forsyth, T. P.; Smith, K. M. *Angew. Chem., Int. Ed. Engl.* **1993**, *32*, 750.
(30) Paolesse, R.; Pandey, R. K.; Forsyth, T. P.; Jacquinod, L.; Gerzevske, K. R.; Nurco, D. J.; Senge, M. O.; Licoccia, S.; Boschi, T.; Smith, K. M. *J. Am. Chem. Soc.* **1996**, *118*, 3869.
(31) Clement, T. E.; Nurco, D. J.; Smith, K. M. *Inorg. Chem.* **1998**, *37*, 1150.
(32) Crossley, M. J.; Mackay, L. G.; Try, A. C. *J. Chem. Soc., Chem. Commun.* **1995**, 1925.

(33) Naruta, Y.; Sasayama, M.; Ichihara, K. *J. Mol. Catal. A* **1997**, *117*, 115.
(34) De Schryver, F. D.; Collart, P.; Vanderdriessche, J.; Goedeweeck, R.; Swinnen, A.; Van der Auweraer, M. *Acc. Chem. Res.* **1987**, *20*, 159.
(35) Lindsey, J. S.; Delaney, J. K.; Mauzerall, D. C.; Linschitz, H. *J. Am. Chem. Soc.* **1988**, *110*, 3610.
(36) Hamilton, D. G.; Davies, J. E.; Prodi, L.; Sanders, J. K. M. *Chem. Eur. J.* **1998**, *4*, 608.
(37) Deng, Y.; Chang, C. J.; Nocera, D. G. *J. Am. Chem. Soc*. **2000**, *122*, 410.
(38) Chang, C. J.; Baker, E. A.; Pistorio, B. J.; Deng, Y.; Loh, Z.-H.; Miller, S. E.; Carpenter, S. D.; Nocera, D. G. *Inorg. Chem.* **2002**, *41*, 3102.
(39) Pistorio, B. J.; Chang, C. J.; Nocera, D. G. *J. Am. Chem. Soc.* **2002**, *124*, 7884.
(40) Chang, C. J.; Deng, Y.; Loh, Z.-H.; Nocera, D. G., manuscript submitted.
(41) Bolze, F.; Gros, C. P.; Harvey, P. D.; Guilard, R. *J. Porphyrins Phthalocyanines* **2001**, *5*, 569.
(42) Chang, C. J.; Deng, Y.; Heyduk, A. F.; Chang, C. K.; Nocera, D. G. *Inorg. Chem.* **2000**, *39*, 959.
(43) Chang, C. J.; Yeh, C.-Y.; Nocera, D. G. *J. Org. Chem.* **2002**, *67*, 1403.
(44) Chang, C. J.; Deng, Y.; Shi, C.; Chang, C. K.; Anson, F. C.; Nocera, D. G. *Chem. Commun.* **2000**, 1355.
(45) Chang, C. J.; Deng, Y.; Lee, G.-H.; Peng, S.-M.; Yeh, C.-Y.; Nocera, D. G. *Inorg. Chem.* **2002**, *41*, 3008.
(46) For a recent paper on the singlet excited states of free-base pillared cofacial bisporphyrins, see: Bolze, F.; Gros, C. P.; Drouin, M.; Espinosa, E.; Harvey, P. D.; Guilard, R. *J. Organomet. Chem.* **2002**, *643*−*644*, 89.
(47) Antipas, A.; Gouterman, M. *J. Am. Chem. Soc*. **1983**, *105*, 4896.
(48) Davydov, A. S. *Theory of Molecular Excitons*; McGraw-Hill: New York, 1962.
(49) Gouterman, M.; Holten, D.; Lieberman, E. *Chem. Phys*. **1977**, *25*, 139.
(50) Tran-Thi, T. H.; Lipskier, J. F.; Maillard, P.; Momenteau, M.; Lopez-Castillo, J.-M.; Jay-Gerin, J.-P. *J. Phys. Chem*. **1992**, *96*, 1073.
(51) Kasha, M.; Rawls, H. R.; El-Bayoumi, M. A. *Pure Appl. Chem*. **1965**, *11*, 371.
(52) Gouterman, M. *J. Chem. Phys.* **1960**, *33*, 1523.
(53) Shelnutt, J. A.; Ortiz, V. *J. Phys. Chem*. **1985**, *89*, 4733.
(54) Le Mest, Y.; L'Her, M.; Collman, J. P.; Kim, K.; Hendricks, N. H.; Helm, S. *J. Electroanal. Chem. Interfacial Electrochem*. **1987**, *234*, 277.
(55) Le Mest, Y.; L'Her, M.; Kim, K.; Hendricks, N. H.; Collman, J. P. *Inorg. Chem*. **1992**, *31*, 835.
(56) Hunter, C. A.; Sanders, J. K. M. *J. Am. Chem. Soc*. **1990**, *112*, 5525.
(57) Scheidt, W. R.; Lee, Y. J. *Struct. Bonding (Berlin)* **1987**, *64*, 1.
(58) Andreasson, J.; Zetterqvist, H.; Kajanus, J.; Martensson, J.; Albinsson, B. *J. Phys. Chem. A* **2000**, *104*, 9307.
(59) Antipas, A.; Gouterman, M. *J. Am. Chem. Soc*. **1983**, *105*, 4896.
(60) The relative magnitudes of the T_1-S_0 energy gaps for Pd_2(DPX) and Pd_2(DPD) were confirmed by DFT calculations, which gave $E(T_1-S_0)$ values of 1.96 and 1.81 eV for Pd_2(DPX) and Pd_2(DPD), respectively.
(61) Knyukshto, V.; Zenkevich, E.; Sagun, E.; Shulga, A.; Bachilo, S. *Chem. Phys. Lett.* **1988**, *297*, 97.
(62) Engelman, R.; Jortner, J. *Mol. Phys*. **1970**, *18*, 145.
(63) Freed, K. F.; Jortner, J. *J. Chem. Phys.* **1970**, *52*, 6272.
(64) Jortner, J.; Bixon, M. *Ber. Bunsen-Ges. Phys. Chem*. **1995**, *99*, 296.
(65) Freed, K. F. *Acc. Chem. Res*. **1978**, *11*, 74.
(66) Casper, J. V.; Meyer, T. J. *J. Phys. Chem.* **1983**, *87*, 952.
(67) Kober, E. M.; Casper, J. V.; Lumpkin, R. S.; Meyer, T. J. *J. Phys. Chem*. **1986**, *90*, 3722.
(68) Bowman, M. K. *Chem. Phys. Lett.* **1977**, *48*, 17.
(69) Tait, C. D.; Holten, D. *Photobiochem. Photobiophys.* **1983**, *6*, 201.
(70) Gentemann, S.; Medforth, C. J.; Forsyth, T. P.; Nurco, D. J.; Smith, K. M.; Fajer, J.; Holten, D. *J. Am. Chem. Soc.* **1994**, *116*, 7363.
(71) Gentemann, S.; Nelson, N. Y.; Jacquinod, L.; Nurco, D. J.; Leung, S. H.; Medforth, C. J.; Smith, K. M.; Fajer, J.; Holten, D. *J. Phys. Chem. B* **1997**, *101*, 1247.
(72) Chirvony, V. S.; van Hoek, A.; Galievsky, V. A.; Sazanovich, I. V.; Schaafsma, T. J.; Holten, D. *J. Phys. Chem. B* **2000**, *104*, 9909.
(73) Sazanovich, I. V.; Galievsky, V. A.; van Hoek, A.; Schaafsma, T. J.; Malinovskii, V. L.; Holten, D.; Chirvony, V. S. *J. Phys. Chem. B* **2001**, *105*, 7818.
(74) Deng, Y. Ph.D. Thesis, Michigan State University, East Lansing, MI, 1997.
(75) Abraham, R. J.; Jackson, A. H.; Kenner, G. W.; Warburton, D. *J. Chem. Soc*. **1963**, 853.
(76) Chong, R.; Clezy, P. S.; Liepa, A. J.; Nichol, A. W. *Aust. J. Chem*. **1969**, *22*, 229.
(77) Buchler, J. W. In *The Porphyrins*; Dolphin, D., Ed.; Academic Press: New York, 1978; Vol. 1, Part A, p 407.
(78) Gray, T. G.; Rudzinski, C. M.; Meyer, E. E.; Holm, R. H.; Nocera, D. G., manuscript submitted.
(79) Harriman, A. *J. Chem. Soc., Faraday Trans. 1* **1980**, *76*, 1978.
(80) Durham, B.; Caspar, J. V.; Nagle, J. K.; Meyer, T. J. *J. Am. Chem. Soc*. **1982**, *104*, 4803.
(81) *ADF2000.02*; Vrije Universiteit Amsterdam: Amsterdam, The Netherlands, 1999.
(82) Baerends, E. J.; Ellis, D. E.; Ros, P. *Chem. Phys.* **1973**, *2*, 41.
(83) Te Velde, G.; Bickelhaupt, F. M.; Baerends, E. J.; Fonseca Guerra, C.; Van Gisbergen, S. J. A.; Snijders, J. G.; Ziegler, T. *J. Comput. Chem.* **2001**, *22*, 931.
(84) Becke, A. D. *Phys. Rev. A* **1988**, *38*, 3098.
(85) Lee, C.; Yang, W.; Parr, R. G. *Phys. Rev. B* **1988**, *37*, 785.
(86) van Lenthe, E.; Baerends, E. J.; Snijders, J. G. *J. Chem. Phys*. **1993**, *99*, 4597.
(87) van Lenthe, E.; van Leeuwen, R.; Baerends, E. J.; Snijders, J. G. *Int. J. Quantum Chem.* **1996**, *57*, 281.
(88) van Lenthe, E.; Ehlers, A.; Baerends, E. J. *J. Chem. Phys.* **1999**, *110*, 8943.